Summary declaration of interest statement

Manuscript title: "Freeze-extraction microporous electroactive supports for cell culture"

Authors in order of authorship: Rosa M. Morales-Román[1], Maria Guillot-Ferriols[1], Laura Roig-Pérez[1], Senentxu Lanceros-Mendez[2,3,4], Gloria Gallego Ferrer[1,5], José Luis Gómez Ribelles[1,5]

Affiliations:

[1]*Centre for Biomaterials and Tissue Engineering (CBIT), Universitat Politècnica de València, Camino de Vera s/n, 46022 Valencia, Spain.*

[2]*Centre/Department of Physics, Universidade Do Minho, Rua da Universidade, 4710-057 Braga, Portugal*

[3]*BCMaterials, UPV/EHU Science Park s/n, 48940 Leioa, Spain*

[4]*IKERBASQUE, Basque Foundation for Science, María Díaz de Haro 3, 48013 Bilbao, Spain.*

[5]*Biomedical Research Networking Centre in Bioengineering, Biomaterials and Nanomedicine (CIBER-BBN), Spain*

Declarations of interest:

None

Freeze-extraction microporous electroactive supports for cell culture

Rosa M. Morales-Román[1], Maria Guillot-Ferriols[1], Laura Roig-Pérez[1],

Senentxu Lanceros-Mendez[2,3,4], Gloria Gallego Ferrer[1,5], José Luis Gómez Ribelles[1,5]

[1]*Centre for Biomaterials and Tissue Engineering (CBIT), Universitat Politècnica de València, Camino de Vera s/n, 46022 Valencia, Spain.*

[2]*Centre/Department of Physics, Universidade Do Minho, Rua da Universidade, 4710-057 Braga, Portugal*

[3]*BCMaterials, UPV/EHU Science Park s/n, 48940 Leioa, Spain*

[4]*IKERBASQUE, Basque Foundation for Science, María Díaz de Haro 3, 48013 Bilbao, Spain.*

[5]*Biomedical Research Networking Centre in Bioengineering, Biomaterials and Nanomedicine (CIBER-BBN), Spain*

Abstract

Poly(vinylidene fluoride) (PVDF) is a semycrystalline polymer with four crystalline phases, of which the all trans conformation (β-phase) is the one with the largest piezoelectric response and best electroactive properties. This smart material is able to reproduce physiological events such as inherent bone piezoelectricity, making it a perfect candidate to drive the osteogenic differentiation of mesenchymal stem cells (MSCs) towards the osteogenic lineage. The influence of topography on the adhesion, proliferation and maintenance of multipotency of this type of cell is well established and has confirmed that the production of variable porosity substrates is a suitable approach for cell therapy. In this work, novel PVDF microporous membranes in the β-phase were developed by the freeze-extraction technique. Membranes with different grades of porosity were obtained by varying the concentration of PVDF in the solution. The cell culture supports thus produced were found to possess good crystallinity, β-phase presence and membrane stiffness. Porcine bone marrow mesenchymal stem cells (pBM-MSCs) were used to study cell adhesion and proliferation. Regarding cell adhesion at 24h, the cells preferred the more porous structures and had round focal adhesions with well-developed cytoskeletons, while they had a round morphology on the less porous membranes. The cells preferred the less porous membranes to proliferate, even though the initial morphology at 24h showed poor adhesion. These findings confirm that the controlled microporosity of β-phase

PVDF membranes can be produced by freeze extraction and offer the possibility of modifying the adhesion and proliferation of pBM-MSCs on these substrates.

Keywords

Poly(vinylidene fluoride); Freeze extraction; Mesenchymal stem cell; Tissue engineering

1. Introduction

Poly(vinylidene fluoride) (PVDF) is a semicrystalline polymer able to form four different crystalline structures, known as α, β, γ and δ. Its piezoelectric properties are due to the net permanent dipole of the polymer chain, which is at a maximum when the polymer chain adopts the all trans conformation in the crystalline β-phase [1], the electroactive phase in which it has the largest piezoelectric response. PVDF has been proposed as a cell culture substrate in the form of bulk or porous films [2][3][4]. In this application, electroactive PVDF films are able to electro-mechanically stimulate cells cultured in monolayer adhering to the film substrate surface, since the application of a dynamic deformation (e.g. sinusoidal) to the film induces the appearance of a dynamic surface electrical charge density due to the piezoelectric effect. In a similar way, the application of a dynamic electric field induces the deformation of the substrate. It has been shown that the electro-mechanical stimulation of cells with osteogenic capacity (mesenchymal stem cells or pre-osteoblasts) significantly influences cell proliferation, viability and differentiation of the substrate [5][6].

Obtaining controlled film substrate porosity is of great interest since it allows the controlled delivery of chemically significant substances to the cells, or even a paracrine interaction between different cell types in co-cultures without any contact. Porous PVDF structures have been produced by different membrane-formation techniques, such as air-casting of the polymer solution, precipitation from the vapour phase, and thermally induced phase separation (TIPS) [7]. Solid-liquid and liquid-liquid phase separation during controlled solvent evaporation have produced micro-porous membranes with well-interconnected porosity [8][9][10]. Techniques incorporating porogens have also been used to produce macro-porous PVDF scaffolds for 3D cell culture [11].

One of the key issues in obtaining PVDF electroactive supports is the crystalline ordering induced by processing. Crystallization from the melt preferably induces crystallization in the

α-phase [12][13], while the β-phase is formed by uniaxial or biaxial deformation of a film in the α-phase [14][15], but also by casting from particular solvents such as dimethyl formamide (DMF), among others [16]. This is why porous PVDF systems obtained by controlled DMF evaporation, mentioned above, were electroactive, and also electrospun PVDF mats obtained from solutions in solvent mixtures containing DMF also present a large fraction of the β-phase [17].

In this work microporous PVDF membranes were produced by freeze-extraction. This technique has been used in the past to produce microporous materials, in particular macro-porous scaffolds, in which the pore walls are in turn microporous [18][19]. The biological response to the particular microtopography of the support surfaces obtained by freeze-extraction has previously been studied in different systems [20].

The aim of this paper is to describe the freeze-extraction procedure used to obtain novel electroactive PVDF supports with controlled microporosity. This method can produce a variety of 3D structures with the polymer crystallized in the electroactive β-phase with precise control of the surface microtopography.

The influence of nanotopographycal niche cues on the signaling pathways induced in stem cells is well established [21]. The influence of nanotopography on the adhesion, proliferation and maintenance of multipotency in mesenchymal stem cells has received special attention [22]. The influence of substrate topography on the micron or submicron scale on MSC adhesion and differentiation has also been clearly demonstrated. The orientation of electrospun fibers can strongly influence MSC differentiation [23][24][25] . The density of electrosprayed microspheres adhering to a flat surface influences cell adhesion, morphology and preservation of multipotency [26]. As the effect of substrate microporosity has received less attention, it is difficult to reach general conclusions, due to the different responses obtained from cells cultured on microporous substrates with different chemistries [27][28][29][30][31]. In this work we analyze the adhesion and proliferation of porcine bone marrow mesenchymal stem cells (pMSCs) on new PVDF supports with different porosities and compliance prepared by the freeze-extraction method. To our knowledge this is the first time that this technique has been used to produce electroactive PVDF membranes for cell stimulation.

2. Materials and Methods

2.1. Membranes by freeze-extraction

Low molecular weight poly(vinylidene fluoride) with (*Mw=352.000, Solef® 1010 PVDF Homopolymer, Solvay*) was dissolved in dimethylformamide (Synthesis grade, Scharlab) at three different concentrations, 10 % w/v (PVDF10), 15 % w/v (PVDF15) and 20 % w/v (PVDF20). The solutions were stirred and heated to different temperatures for different times to completely dissolve the polymer and avoid the "yellowing effect" caused by secondary reactions. Fresh solutions of PVDF10, PVDF15 and PVDF20 were stirred at 40, 45 and 50 °C for 60, 90 and 120 minutes, respectively.

Freeze-extraction is a two-step technique, including the initial freezing of the solution in which crystallization of both PVDF and DMF takes place, with the subsequent extraction of the solvent at temperatures below the DMF and PVDF melting point (−61 °C), maintaining the structure of the polymer formed during freezing. In the first step of this method, the PVDF solution was poured into a Petri glass dish coated with a poly(vinyl alcohol) (PVA) layer, obtained by previous solvent-casting of a PVA 10 % w/v solution (Sigma) on the plate, to assist in the subsequent detachment of the membrane and prevent it from breaking up. The uncovered plate was immediately placed in an airtight container, to which 15 mL of DMF were added to saturate the atmosphere containing the PVDF solution with DMF vapor, thus preventing evaporation of the solvent before freezing, since this would create a non-porous skin on the membrane. The container was then frozen to -80ºC.

The solution in the container was kept in the freezer for 60, 90 and 120 minutes for PVDF10, PVDF15 and PVDF20, respectively, and transferred to a pre-cooled vessel at -80ºC with 300 mL of absolute ethanol to begin DMF removal. The entire extraction process was performed at -80ºC in static conditions to maintain the PVDF microstructure achieved during freezing.

After four washes with pre-cooled ethanol, the membranes were thawed slowly on ice to avoid sudden changes in temperature. Quick solvent exchanges, rapid solvent evaporation or sudden changes in temperature tend to bend the membrane or collapse the pore structure. Homogeneous membranes suitable for physical and biological assays were obtained when the ethanol from the washings, which fills the pores, is gradually exchanged by adding dropwise double the volume of distilled water in the initial volume of ethanol.

The remaining traces of ethanol were eliminated by washing with distilled water for 2 days. The membranes were frozen and lyophilized for 24 hours.

2.2. Electroactive PVDF films

PVDF films in the β-phase were used as controls for the cell culture evaluation. They were obtained by pressing PVDF15 membranes at 200 bar and 140 °C for 3 minutes with a hot press (TP-250/200/1-E, Gumix) followed by rapid cooling.

2.3. Material Characterization

Scanning Electron Microscopy and Field Emission Scanning Electron Microscopy

The surface structure of the PVDF10, PVDF15 and PVDF20 membranes was analysed by Scanning Electron Microscopy (SEM) on a JEOL JSM 6300 microscope at an accelerating voltage of 10 kV. The samples were stuck to copper supports by carbon tape, with a carbon bridge from the observed surface to the copper support to ensure conductivity. They were then coated with gold following a standard sputtering protocol for 90 seconds (JFC 1100, JEOL, Japan). The cross-section was visualized by Field Emission Scanning Electron Microscopy (FESEM) at 1 kV in samples coated with platinum for 90 seconds. The surface of the film was visualized by FESEM following the same protocol.

Porosity

The porosity of the membranes was calculated by filling the pores with ethanol and applying Eqs. 1 and 2

Eq. 1 $$V_{pores} = \frac{m_{wet} - m_{dry}}{\rho_{liquid}}$$

Eq. 2 $$\phi = \frac{V_{pores}}{(V_{pores} + V_{PVDF})}$$

Where m_{dry} and m_{wet} are the weight of the membrane before and after immersion, respectively, ρ_{liquid} is the ethanol density and V_{PVDF} is the polymer volume at a density of 1.775 $g \cdot cm^{-1}$.

Fourier-Transformed Infrared Spectroscopy (FTIR)

The piezoelectric property of the membrane and film was verified by the presence of the most representative absorption bands of the electroactive β-phase at 840 and 510 cm^{-1} and the minimum appearance or absence of α-phase peaks (614, 765, 795 y 976 cm^{-1}) in the entire scan of the IR spectra at a wavelength resolution of 4 cm^{-1} (ALPHA FT-IR spectrometer, Bruker). The spectras were compared with that of the raw material.

Equation 3 was used to determine the α and β-phase content in the processed PVDF samples [1][16]. Given a sample containing α or β-phase only, assuming that FTIR absorption follows the Lambert-Beer law and at given absorption coefficients, K_α and K_β, at the characteristic wavenumbers of the α and β-phases (765 and 840 cm^{-1}, respectively), the β-phase fraction is:

Eq.3
$$F(\beta) = \frac{A_\beta}{\left(K_\beta / K_\alpha\right) A_\alpha + A_\beta}$$

Where $F(\beta)$ represents the β-phase content; A_α and A_β the absorbance at 765 and 840 cm^{-1}; K_α and K_β are the absorption coefficients for the cited wave numbers, whose values are 6.1×10^4 and 7.7×10^4 $cm^2 mol^{-1}$, respectively.
The spectra were treated by ambiental baseline subtraction and Min-Max normalization.

Differential Scanning Calorimetry (DSC)

The thermal properties of the material were analyzed by differential scanning calorimetry in a dry nitrogen atmosphere. The experiments were carried out in sealed aluminum pans with a DSC Pyris 1 (Perkin-Elmer) in a temperature range from -80 °C to 200 °C with cooling and heating scans at a rate of 20 °C/min. The sample weight ranged between 4 and 10 mg. The degree of sample crystallinity was determined by Eq. 4, where ΔH_m is the enthalpy of the melting peak of the sample, x and y are the content of α and β-phase obtained using Eq.3, and ΔH_α and ΔH_β are the melting enthalpies for a 100% crystalline sample in the α and β-phase, respectively [15]

Eq. 4
$$\Delta X_c = \frac{\Delta H_m}{x\Delta H_\alpha + y\Delta H_\beta}$$

Dynamic Mechanical Analysis (DMA)

The temperature dependence of the elastic modulus was measured by applying a 1 Hz sinusoidal deformation of 0.05 mm amplitude in a Perkin Elmer DMA8000. Elastic modulus measurements were taken from five replicas for each type of membrane from 32 °C to 90 °C at a heating rate of 2 °C/min. The samples used were around 5 mm wide, 10 mm long and 1 mm thick.

2.4. Cell culture

Porcine mesenchymal bone marrow stem cells were used to conduct all the tests. The cells were expanded in a basal medium containing Dulbecco's modified Eagles medium (DMEM), high glucose (4,5 g/L) with GlutaMAXTM (Gibco), 10% (v/v) Fetal Bovine Serum, FBS (Gibco), 100 U/mL Penicillin/Streptomycin, P/S (Life technologies), and 5ng/mL of Fibroblast Growth Factor 2, FGF-2 (Eurobio), at 37ºC in a humidified atmosphere with 5% CO_2. All the experiments were performed in passages 3-4.

The different types of samples in the form of 8 mm diameter disks were sterilized by different methods. PVDF membranes were irradiated with gamma radiation (25 kGy dosage) due to their porosity. PVDF films were sterilized by disinfection with several antibiotic solutions, followed by 30 min of UV light exposure on each side. The glass slides used as a positive cell control were cleaned and sterilized by a combination of ethanol washes and UV light. Due to the high hydrophobicity of PVDF, porous membranes were immersed in DPBS under vacuum to ensure material sinking. All PVDF samples and controls were coated with fibronectin by incubation of a 20 µg/mL solution (Sigma-Aldrich) on the seeding surface for 1 hour at room temperature.

Cell adhesion

For the adhesion study, the cells were seeded (3 replicates per group) at a density of 2×10^4 cells/cm^2 in basal medium without FBS to promote cell adhesion to fibronectin. After 3 hours the required volume of FBS for a final concentration of 10% v/v was added to each well. The cells were cultured at 37ºC in a humidified atmosphere with 5% CO_2 for 24 h and then fixed in a 4% paraformaldehyde solution (Panreac) for 20 minutes.

An immunofluorescence technique was used to determine the correlations between the material microstructure and cell adhesion and morphology by means of a mouse monoclonal primary antibody anti-vinculin (1:300, Millipore). After overnight incubation at 4ºC, the samples were

incubated with the secondary antibody goat anti-mouse Alexa Fluor 555 (1:100, Invitrogen) and Alexa Fluor 488 Phalloidin (1:75, Life Technologies) for 2 hours. All the samples were then treated with a specific Sudan Black B (Sigma-Aldrich) staining protocol based on information obtained from the literature. The samples were then immersed in a solution of Sudan Black B 0.1% (w/v) in ethanol 70% (v/v) for 20 min with gentle stirring and washed 3 times in DPBS to remove staining excess. Sudan Black treatment was performed to avoid PVDF autofluorescence, which hinders image acquisition and quantification [32][33]. Finally, 2-(4-amidinofenil)-1H-indol-6-carboxamidina (DAPI, 1:400, Sigma-Aldrich) was added to the mounting medium to stain the cell nuclei. Images of four representative fields from each sample were taken by fluorescence microscope (Nikon Eclipse 80i) and analyzed on Fiji-Image J software.

Cell proliferation

For the proliferation assay, using the same protocol as in the adhesion study, the cells were seeded at a density of 1×10^4 cells/cm^2. The proliferation rate was measured at three different times: 24 hours, 3 days and 7 days.

To determine any differences in cell proliferation due to the material, the cells were counted by nucleus and cytoplasm fluorescent staining (3 replicates per group).

For cell number quantification, the cells were stained with fluorescent dyes to mark the cell nucleus with 1:400 dilution of DAPI (Sigma-Aldrich) solution and actin microfilaments with a 1:75 dilution of Alexa Fluor 488 Phalloidin (Life Technologies). As in the adhesion study, the samples were treated with Sudan Black B to avoid PVDF autofluorescence. Four photos were taken per sample from four representative areas with a Fluorescence Microscope (Nikon Eclipse 80i). The images were analyzed by Fiji Image J software and cell numbers were counted per mm^2.

Cell Circularity

Fiji ImageJ shape descriptors were also used for a quantitative study of cell morphology at 24 hours in the adhesion study and at 3 days in the proliferation study. Briefly, masks of images were obtained by previous segmentation and the circularity measurements for the scaled images were taken. The circularity parameter is defined by Eq. 5:

Eq. 5
$$Circularity = \frac{4 \cdot Area}{\pi \cdot (Perimeter)^2}$$

The index of circularity was obtained for the cells of 4 representative areas in each biological replica. Data were obtained from two or three biological replicas for the adhesion and proliferation studies, respectively.

2.5. Statistical analysis

A statistical analysis was performed on Graphpad Prism 7 software (Graphpad Software, United States). For circularity and cell counting data, one-way or two-way ANOVA analysis was applied to homogeneous groups with normal distributions, confirmed by a Levene's test on SPSS software. The Kruskal-Wallis non-parametric test was used for non-homogeneous groups. Significance was accepted as $p\text{-value} < 0.05$.

3. Results and Discussion

3.1. Physico-chemical properties of the membranes

PVDF membranes were produced from the DMF solution, since it has been shown that the β phase can be formed by casting from this solution. In the first step of freeze-extraction, the solution is frozen with variable polymer content, which makes both PVDF and DMF solidify and phase separate. In PVDF domains the amorphous and crystalline phases coexist. DMF is then dissolved at a temperature below its melting point, thus avoiding the formation of liquid DMF, which would be absorbed by the polymer and affect its structure. Since the melting point of DMF is -61ºC, extraction was performed at -80ºC with ethanol. At the end of this stage the pores of the PVDF membrane are filled with pure ethanol. The key issue in the formation of the porous membrane is that the conformational mobility of the PVDF chains be arrested during the whole process. As we will discuss below in more detail, molecular mobility is enhanced by the absorption of even small amounts of a low molecular weight substance, or when the temperature rises. At -80ºC the amount of ethanol absorbed by PVDF seems to be negligible and the volume of the sample is practically the same as the original PVDF solution in DMF. If the temperature increases in these conditions to around room temperature the increase of conformational mobility due to ethanol absorption allows the polymer to rearrange and the pore collapses with a significant reduction of membrane volume. To avoid this undesirable effect, ethanol is exchanged for water, since PVDF is highly hydrophobic and only absorbs a negligible amount of water.

Finally, the sample is dried in a vacuum. The microstructure of the surface for samples obtained from PVDF solutions containing 10, 15 and 20 % polymer by weight and the cross-sectional

membrane microstructure for PVDF15 are shown in Figure 1. Interestingly enough, the membranes are formed by the aggregation of PVDF microspheres and although they are mechanically consistent, their mechanical characterization will be shown below. Microsphere diameters are nearly monodisperse in all three membranes, with a mean diameter in μm that increases with the PVDF concentration in the starting solution: 0.42±0.08/ 0.55±0.10/ 0.88±0.18 in the series PVDF10/PVDF15/PVDF20 (Table 1). This structure is of a spherulitic growth of the PVDF crystals from the solution during cooling. Each microsphere shown in Figure 1 is from a single spherulite. The larger the amount of polymer in the solution, the larger the diameter of the spherulite, since growth only stops when the polymer chains are exhausted in the neighboring solution. PVDF crystal growth seems to be independent of that of DMF, which can be explained by the DMF's low melting point. PVDF solidifies on cooling before the start of DMF crystallization.

Table 1.- Physical properties of PVDF membranes

	Porosity (%)	Microbead diameter (μm)	Number of microbeads per mL	Elastic modulus E' at 37 ºC (MPa)
PVDF10	84.2±0.4	0.42±0.08	4.07×10^{12}	5.65±2.50
PVDF15	81.7±0.9	0.55±0.10	2.10×10^{12}	14.63±2.55
PVDF20	80.1±1.7	0.88±0.18	5.58×10^{11}	46.42±14.26

Table 2.- Contraction of PVDF membrane after heat treatment

	Volume reduction after heating (%)	Thickness reduction after heating (%)
PVDF10	24.11±5.61	11.35±3.71
PVDF15	14.39±1.62	4.91±1.69
PVDF20	20.22±2.40	6.16±2.43

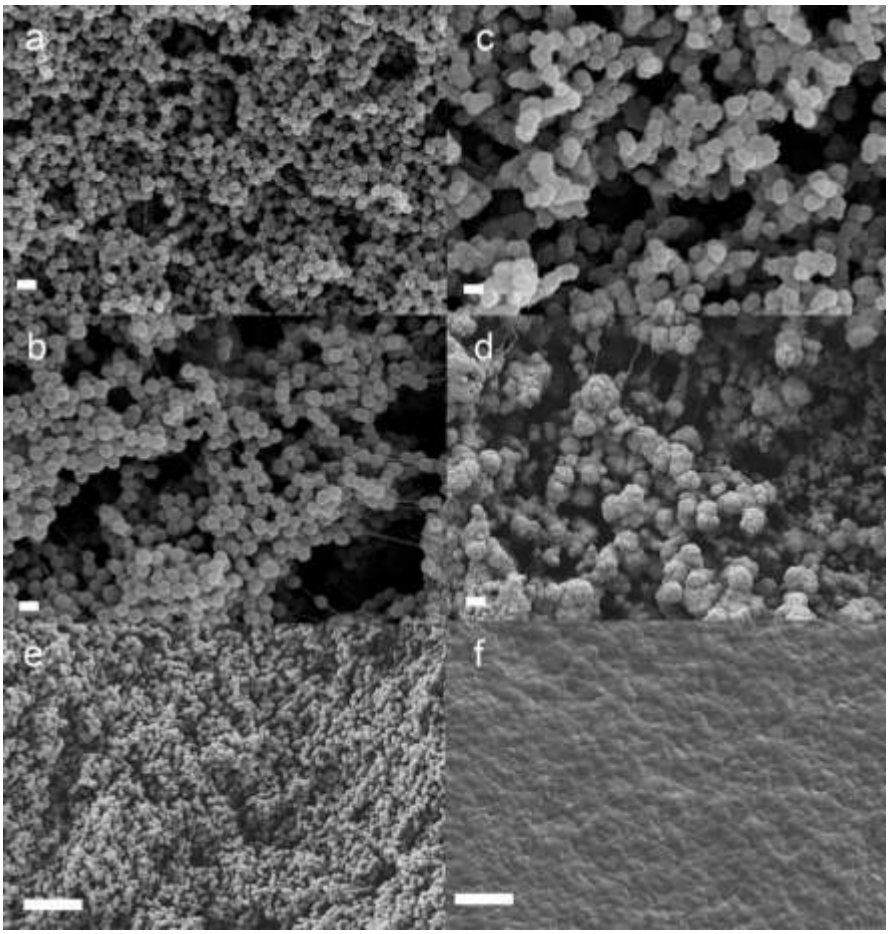

Figure 1. SEM pictures of the surface of (a) PVDF10 (b) PVDF15 and (c) PVDF20 membranes. Picture (d) shows sample PVDF20 after heating to 80ºC. (e) Cross-section of PVDF15 membrane. (f) Surface of PVDF film. The dimension bar corresponds to 1 μm for (a), (b), (c) and (d) and 10 μm for (e) and (f).

Porosity was determined by filling the pores of the membrane with ethanol in a vacuum (the values are shown in Table 1). Mean porosity decreases with increasing PVDF content in the original solution in DMF. It should be noted that if the same procedure is followed with water instead of ethanol, the pore volume is underestimated (values of 77.8±1.8/64.0±4.6/68.0±3.6 in the series PVDF10/PVDF15/PVDF20), which shows the difficulty of filling all the pore structure of the membrane with water, due to PVDF's high degree of hydrophobicity. The mean number of particles per unit volume of the membrane can be determined from the pore volume and the mean diameters of PVDF microspheres. This provides information on the dependence of nucleation on the polymer concentration in the solution. The values found (Table 1) indicate that the lower the concentration of the polymer in the solution, the higher the number of

crystallization nuclei, which could be related to the lower crystallization temperature during the cooling scan.

The β-phase fraction was determined by FTIR. The spectra of all the membranes are similar. In Figure 2, that of PVDF15 is compared with that of a PVDF film and α-phase raw material. Absorption bands at 765, 795, 855 and 976 cm^{-1} are characteristic of the α-phase, while the 840 cm^{-1} band is the main absorption band of the β-phase.

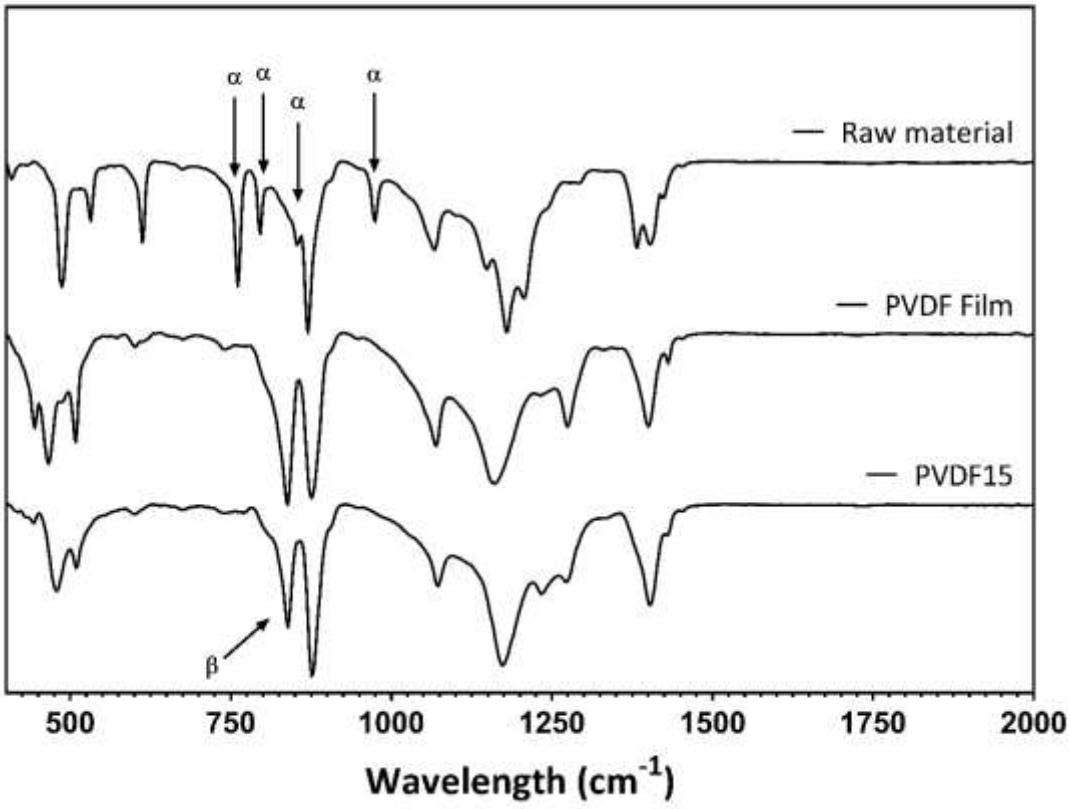

Figure 2. Infrared spectra for the PVDF15 membrane, a β-PVDF film (obtained by pressing membranes PVDF15 at 200 bar and 140 °C, see text) and raw material.

The β-phase content of the membranes was calculated from the infrared absorption bands at 765 cm^{-1} and 840 cm^{-1}, characteristic of the α and β-phases of PVDF, respectively, with a procedure similar to the one described in [16]. Applying Eq.3, the value obtained for F(β) is nearly the same in all the membranes (94%), which clearly shows that cooling-induced crystallization in the solution is highly effective in forming the electroactive β-phase in PVDF membranes.

Interestingly enough, although the microstructure of these membranes appears to be formed by an agglomeration of independent particles, inter-particle adhesion is high enough to give mechanical consistency to the material. The elastic modulus of the membranes was determined by dynamic-mechanical analysis. Figure 3 shows the temperature-dependence of the real part of the elastic modulus (E') measured in tension mode in the temperature interval between 30 and 70ºC. The values of the elastic modulus at 37ºC are listed in Table 1. At lower temperatures the results show that membrane stiffness is considerably reduced with decreasing PVDF concentration in the starting solution in DMF. In this case the higher porosity evidently has an influence, but it should be noted that the difference in the pore fraction is not high enough to justify the change in E'. Inter-particle adhesion thus appears to increase with the concentration of PVDF in the initial solution.

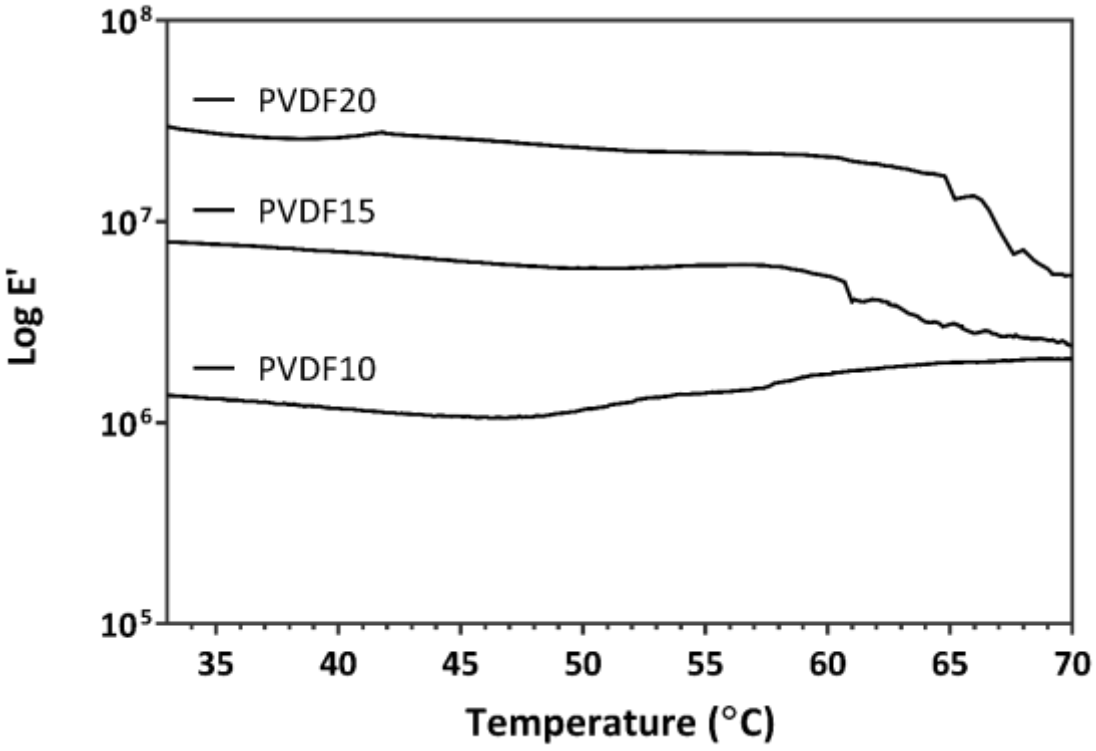

Figure 3. Elastic modulus of PVDF membranes.

The other interesting feature is the contraction of the membrane when PVDF chains acquire enough mobility. As the mechanical properties are strongly dependent on porosity, this technique is highly sensitive to structural changes. The onset of pore collapse in the membrane is characterized by a higher elastic modulus, which otherwise decreases monotonously during a heating scan. This phenomenon can be seen in Figure 3, especially in the PVDF10 sample, and also in PVDF15 and PVDF20. The onset of the rise in E' is detected around 50ºC. After an

initial increase, at higher temperatures the modulus declines in all the samples. The dimensions of the sample were measured to confirm pore collapse before and after the heating scans up to 80ºC.

The percentage volume loss is shown in Table 2, while Figure 1d shows the microstructure of the PVDF20 sample after heating at 80ºC, for comparison with the same sample in Figure 1c before thermal treatment. The increased modulus is more evident in PVDF10, which is the material that lost most volume. On the other hand, PVDF20 lost more volume than PVDF15, although both had similar E' increases at the onset. Considering the reduction in each dimension separately, thickness decreases considerably more in PVDF10 than in the other two materials, as shown in Table 2. The volume reduction in PVDF10 is thus mainly due to its pores collapsing because of higher porosity, while in PVDF15 and PVDF20 it is caused by the internal stresses accumulated during synthesis, which increase with polymer content. Interestingly enough, the onset of contraction coincides with a small endothermic peak in the DSC heating thermograms, shown in Figure 4. The small peak, starting at 50ºC, visible in the first heating scan (Figure 4) disappears in the second (results not shown), with the thermograms being almost identical in the different samples. The main melting peak appears in the same temperature range as in the raw material (Figure 4).

These features can thus be explained by the crystallization process: the growth of the spherulites during cooling requires the diffusion of PVDF chains from the solution to the spherulite surfaces; the spherulites start touching each other only at the end of the process and then they are bonded by the formation of crystal lamellae in the spherulite interphases. These interphase crystals are formed at the later stages of crystallization at the lowest temperatures and consequently they have the lowest melting temperatures. It can therefore be hypothesized that the melting of small crystals at 50ºC reduces inter-particle adhesion and allows the pores to collapse.

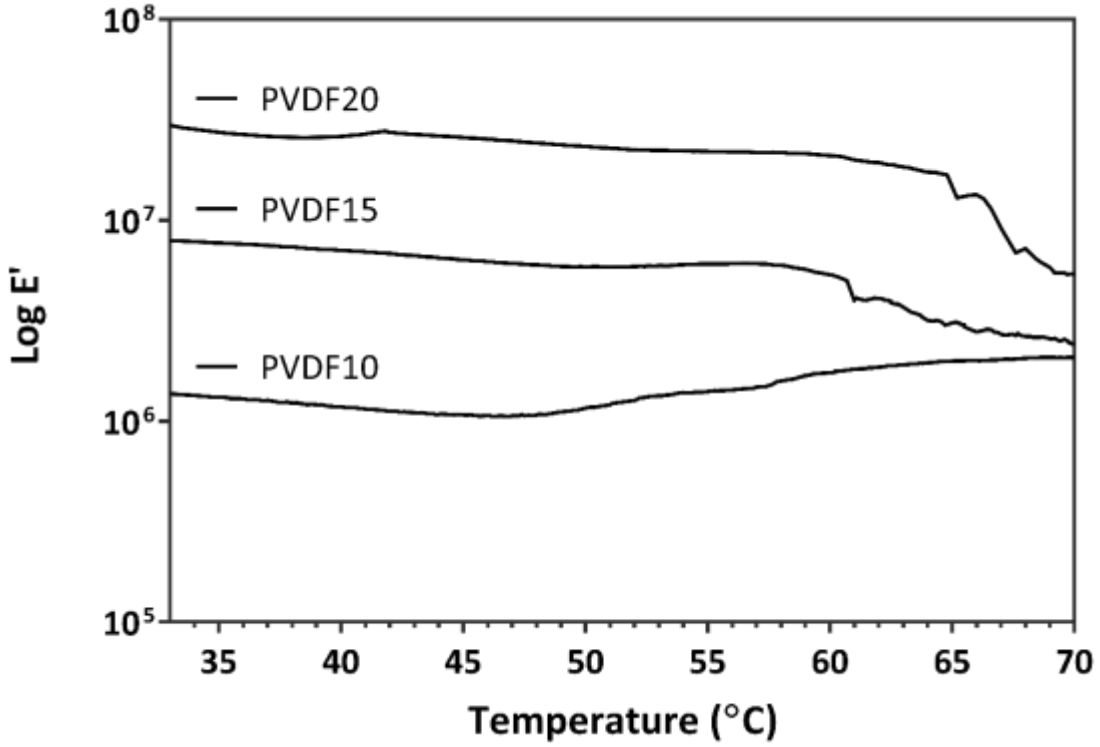

Figure 4. DSC heating thermograms of PVDF membranes and raw material. First scan shows the endothermic peak at around 50ºC before the main melting peak, which is associated with sample contraction and disappears in the second scan.

3.2. Cell culture assays

Cell adhesion to the substrates and proliferation were studied using a PVDF film and a glass support as controls.

The fluorescence microscope images taken 24 hours after seeding show that the adhesion of the cells to the non-porous PVDF film is similar to that of the glass control (Figure 5). It can be seen that these cells take some time to spread out on the substrate and there are large differences between the different membranes. There is a clear expression of vinculin, although the focal adhesion plates cannot be distinguished. Actin stress fibers can be seen in all the cells.

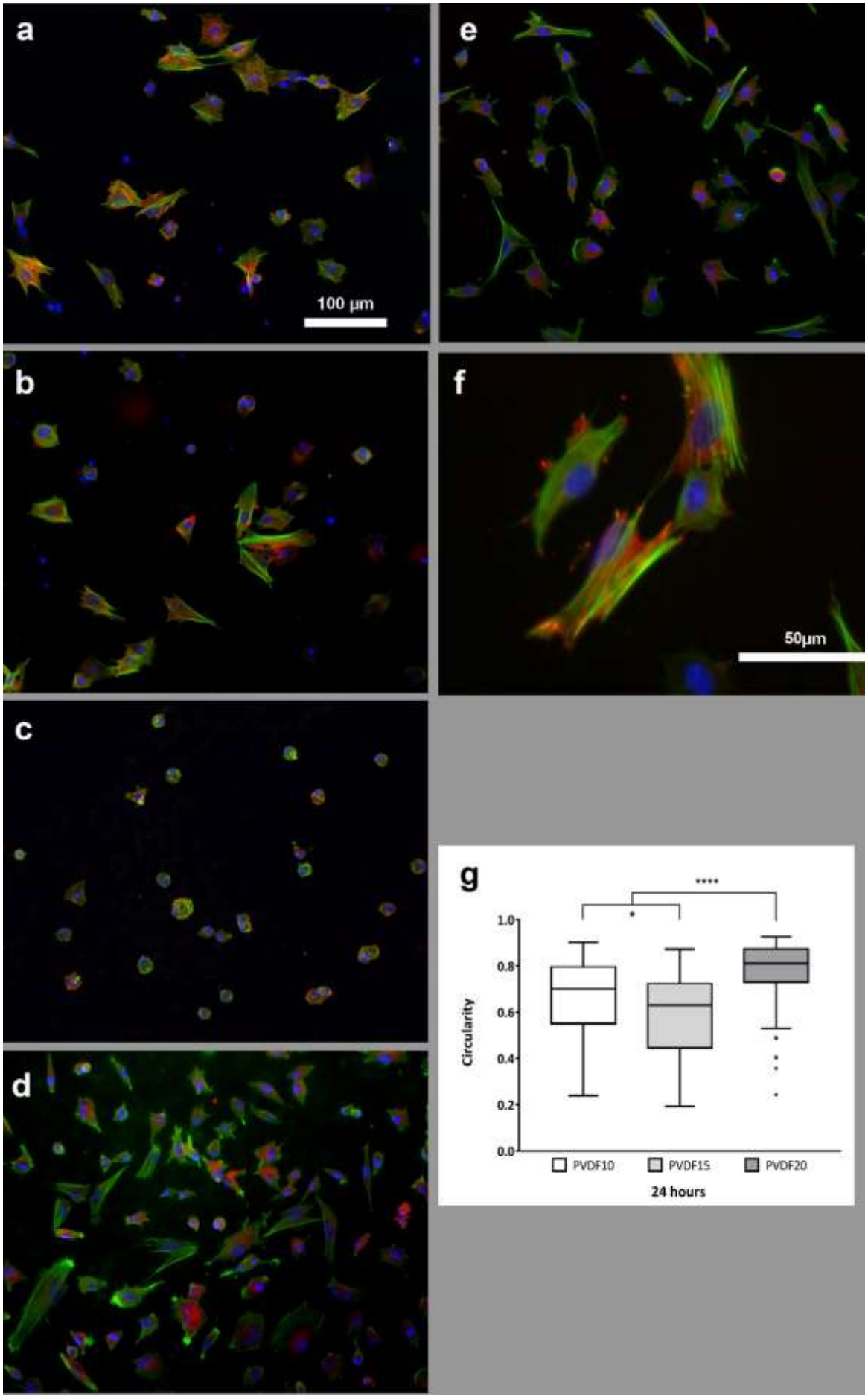
a
100 µm
e
b
f
50µm
c
d
g
****
*
1.0
0.8
0.6
0.4
0.2
0.0
Circularity
PVDF10
PVDF15
PVDF20
24 hours

Figure 5. Images of actin/vinculin immunofluorescence after 24h. Cell nuclei, stained with DAPI are shown in blue, actin cytoskeleton in green and vinculin appears in red. Cell adhesion is shown on (a) PVDF10 (b) PVDF15 (c) PVDF20 (d) PVDF film (e) glass slide. (f) PVDF10 magnification in which round focal adhesions in the shape of PVDF spherulites can be seen. Scale bar shown in (a) is that of 100 μm and is valid for pictures (a) to (e). Scale bar in (f) is that of 50μm. (g) Box-plot of circularity data obtained after 24 hours from the actin/vinculin immunofluorescence pictures.

In the porous membranes cell adhesion clearly depends on porosity, as shown in Figure 5. It is interesting to see that the cells spread out more in the PVDF10 sample, while in PVDF20 after 24 hours the cells have a rounded shape and sizes of the order of 20 microns. In contrast, PVDF15 has a similar behavior to PVDF10 in terms of cell shape and spreading. To support these results, some quantitative parameters were examined in the adhesion study by imaging analysis software. Circularity is an adimensional parameter calculated from cell surface and perimeter, as defined by Eq.5. The nearer the index of circularity is to 1, the rounder the cell.
Figure 5g, shows the tendency to a rounded cell shape at 24 hours and is noticeable in PVDF20, in agreement with the cell adhesion images. The responses to PVDF10 and PVDF15 are slightly different, with more expansion in PVDF15.
In contrast to this initial response, the influence of substrate porosity on cell behavior looks quite different for longer culture times, as shown in Figures 6 and 7. Figure 6 shows images of nuclei stains and the actin cytoskeleton at 7 days in culture. Again, the behavior of the PVDF film and the glass control are quite similar. It can be seen that in the PVDF15 and PVDF20 samples the MSCs also proliferate actively, while in the more porous PVDF10 sample, despite the initial adhesion, the cells are not able to proliferate and even decline in number with the culture time. The circularity index was extracted for the cells cultured for 3 days. The average circularity index for PVDF15 and PVDF20 is lower than for PVDF10, which means a more expanded morphology in PVDF15 and PVDF20. The dispersion of the data in PVDF10 can be highlighted, since it implies a wide range of cell shapes, from which a negative cellular response to the highest porosity substrate with the culture time can be deduced.

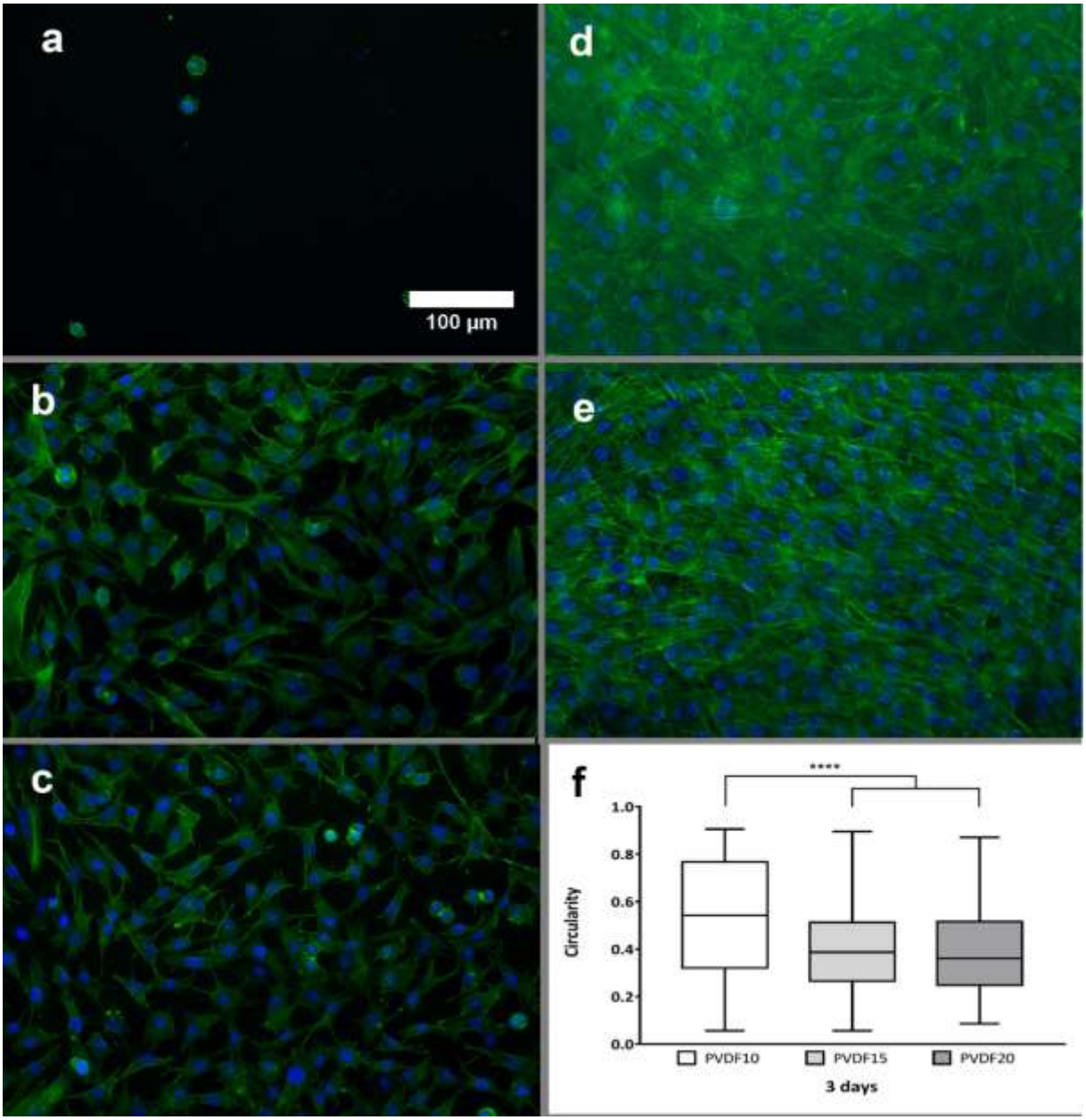

Figure 6. Images of actin/DAPI staining at 7 days. Nuclei appear in blue, actin cytoskeleton in green. Image (a) is of PVDF10, in which almost no cells remain after 7 days, (b) and (c) are those of PVDF15 and PVDF20, with active MSC proliferation, and (d) and (e) are PVDF film and glass slide, respectively. Scale bar shown in (a) is that of 100 µm and is valid for pictures (a) to (e). (f) Box-plot of circularity index for actin/DAPI staining images at 3 days.

The cell counts are shown in Figure 7. The results reflect the impression obtained from the images shown in Figure 6, where it can be seen that the rate of proliferation differs with porosity. MSCs actively proliferate in the less porous supports but at a lower rate than in the controls. According to the results of the ANOVA test there are slightly significant differences between the different membranes at 7 days.

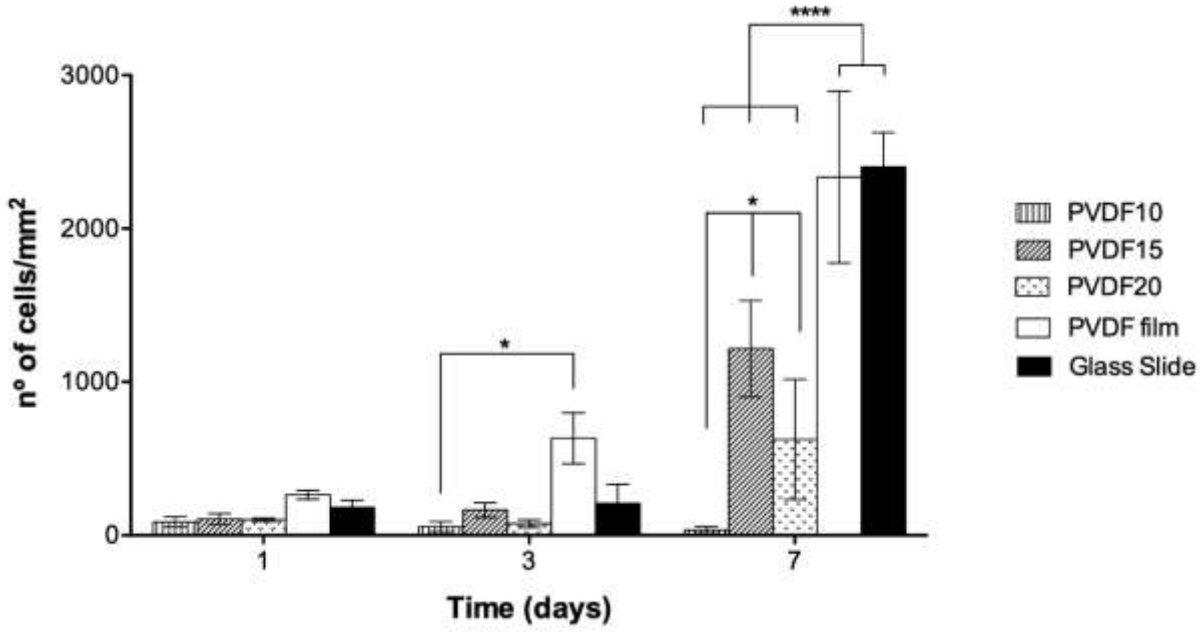

Figure 7. -Cell count based on the analysis of 4 images taken from different areas of three replicas at three different times, 24h, 3 days and 7 days.

It has been reported that MSCs are able to spread in microporous substrates with pores of the order of 1 micron, and even that initial adhesion is enhanced by microporosity, although this result is not general. On the other hand, it has also been found that MSC proliferation is suppressed in different microporous systems. Thus, although human MSCs cultured on polylactide microporous membranes were able to adhere and spread out, proliferation was suppressed while apoptosis significantly increased [20]. In microporous substrates made of bioactive glass, microporosity greatly enhanced initial adhesion and proliferation of rat bone marrow MSCs [31]. Nevertheless, in polystyrene honey-comb scaffolds, with pores in the order of 1 micron, human MSC adhesion was greatly reduced, the cells being smaller and more polygonal than on the flat substrates, and proliferation was also greatly reduced. Interestingly, this effect was less pronounced in supports with the same structure but larger pores, in the order of 10 microns [34]. Also, Collart-Dutilleu et al. cultured human dental pulp stem cells on nanoporous and microporous silicon substrates and found that the initial adhesion of cells to the substrate decreased in supports with 1 micron pores and subsequent proliferation was almost completely suppressed [27].

The influence of surface structure on cell adhesion and proliferation has been found to be related to the formation and maturation of focal adhesions [35]. It has also been shown that topography

increases the amount of protein adsorbed on the surface and that microporosity has a favorable influence on the exhibition of adhesion ligands of collagen [30] or fibronectin [31] adsorbed on the substrate.

The explanation of the high levels of adhesion on PVDF10 samples could be related to PVDF's higher porosity than PVDF15 and PVDF20. Fibronectin adhesion domains would be more exposed to cells on PVDF10 supports, allowing better adhesion during the first 24 hours.

Cell morphology differs from the MSC shapes in the most frequently studied microtopographies: electrospun fibers. On random fibers, MSC show a cellular stellate-like morphology, while on aligned fibers the cells acquire an elongated fibroblast-like shape [25]. On microporous PVDF membranes, the cells show a well spread out morphology, comparable to that of the controls. In our supports they were found to have round focal adhesions (Figure 5f) similar to the PVDF spherulites present on the membrane surface, suggesting that focal adhesions reproduce the shape of the microspheres to which they are adhered. According to Chen et al., cell shape regulates the quantity, size and organization of the focal adhesions mediated by changes in cell contractility governed by the cytoskeleton [36]. The expanded morphology of the cells on the membranes, as shown by the actin fibers, is due to mechanical tension in the cytoskeleton and could be responsible for the rounded focal adhesions.

4. Conclusions

The freeze-extraction method can be used to produce PVDF membranes without skin effects whose porosity depends directly on the concentration of the solution that is frozen in the process. The structure of the membrane consists of an agglomerate of PVDF microspheres sufficiently adhered to one another, so that the membrane is mechanically consistent, and its stiffness depends on the porosity and microstructure of the membrane. The beginning of the melting of the PVDF crystallites at around 50ºC produces a contraction of the membrane by releasing the internal stresses retained in the sample during the freeze extraction process.

MSCs can initially adhere and spread out even in the most porous samples, while the initial cell spreading increases with surface porosity in the range of the samples produced in this study. However, in the most porous samples the MSCs are not able to proliferate, although they can do so actively in the less porous samples.

Acknowledgments

This work was supported by the Spanish Government through Projects MAT2016-76039-C4-1-R and MAT2016-76039-C4-3-R (including FEDER funds). Maria Guillot-Ferriols acknowledges the government funding of her doctoral thesis through a BES-2017-080398FPI Grant. The CIBER-BBN initiative is funded by the VI National R&D&I Plan 2008-2011, *Iniciativa Ingenio 2010*, Consolider Program. CIBER actions are financed by the *Instituto de Salud Carlos III* with assistance from the European Regional Development Fund.

References

[1] P. Martins, A.C. Lopes, S. Lanceros-Mendez, Electroactive phases of poly(vinylidene fluoride): Determination, processing and applications, Prog. Polym. Sci. 39 (2014) 683–706. doi:10.1016/j.progpolymsci.2013.07.006.

[2] M.T. Rodrigues, M.E. Gomes, J.F. Mano, R.L. Reis, β-PVDF Membranes Induce Cellular Proliferation and Differentiation in Static and Dynamic Conditions, Mater. Sci. Forum. 587–588 (2008) 72–76. doi:10.4028/www.scientific.net/MSF.587-588.72.

[3] C. Ribeiro, J.A. Panadero, V. Sencadas, S. Lanceros-Méndez, M.N. Tamaño, D. Moratal, M. Salmerón-Sánchez, J.L. Gómez Ribelles, Fibronectin adsorption and cell response on electroactive poly(vinylidene fluoride) films, Biomed. Mater. 7 (2012) 035004. doi:10.1088/1748-6041/7/3/035004.

[4] P. Hitscherich, S. Wu, R. Gordan, L.H. Xie, T. Arinzeh, E.J. Lee, The effect of PVDF-TrFE scaffolds on stem cell derived cardiovascular cells, Biotechnol. Bioeng. 113 (2016) 1577–1585. doi:10.1002/bit.25918.

[5] C. Ribeiro, S. Moreira, V. Correia, V. Sencadas, J.G. Rocha, F.M. Gama, J.L. Gómez Ribelles, S. Lanceros-Méndez, Enhanced proliferation of pre-osteoblastic cells by dynamic piezoelectric stimulation, RSC Adv. 2 (2012) 11504–11509. doi:10.1039/c2ra21841k.

[6] C. Ribeiro, J. Pärssinen, V. Sencadas, V. Correia, S. Miettinen, V.P. Hytönen, S. Lanceros-Méndez, Dynamic piezoelectric stimulation enhances osteogenic differentiation of human adipose stem cells, J. Biomed. Mater. Res. - Part A. 103

(2015) 2172–2175. doi:10.1002/jbm.a.35368.

[7] C. Ribeiro, C.M. Costa, D.M. Correia, J. Nunes-Pereira, J. Oliveira, P. Martins, R. Gonçalves, V.F. Cardoso, S. Lanceros-Méndez, Electroactive poly(vinylidene fluoride)-based structures for advanced applications, Nat. Protoc. 13 (2018) 681–704. doi:10.1038/nprot.2017.157.

[8] V.-T. Bui, V.-D. Dao, H.-S. Choi, Transferable thin films with sponge-like porous structure via improved phase separation, Polymer. 101 (2016) 184–191. doi:10.1016/J.POLYMER.2016.08.063.

[9] R. Magalhães, N. Durães, M. Silva, J. Silva, V. Sencadas, G. Botelho, J.L. Gómez Ribelles, S. Lanceros-Méndez, The role of solvent evaporation in the microstructure of electroactive β-poly(vinylidene fluoride) membranes obtained by isothermal crystallization, Soft Mater. 9 (2011) 1–14. doi:10.1080/1539445X.2010.525442.

[10] A. California, V.F. Cardoso, C.M. Costa, V. Sencadas, G. Botelho, J.L. Gómez-Ribelles, S. Lanceros-Mendez, Tailoring porous structure of ferroelectric poly(vinylidene fluoride-trifluoroethylene) by controlling solvent/polymer ratio and solvent evaporation rate, Eur. Polym. J. 47 (2011) 2442–2450. doi:10.1016/j.eurpolymj.2011.10.005.

[11] D.M. Correia, C. Ribeiro, V. Sencadas, L. Vikingsson, M. Oliver Gasch, J.L. Gómez Ribelles, G. Botelho, S. Lanceros-Méndez, Strategies for the development of three dimensional scaffolds from piezoelectric poly(vinylidene fluoride), Mater. Des. (2016) 674-681. doi:10.1016/j.matdes.2015.12.043.

[12] P. Sajkiewicz, Crystallization behaviour of poly(vinylidene fluoride), Eur. Polym. J. 35 (1999) 1581–1590. doi:10.1016/S0014-3057(98)00242-0.

[13] V. Sencadas, C.M. Costa, J.L. Gómez Ribelles, S. Lanceros-Mendez, Isothermal crystallization kinetics of poly(vinylidene fluoride) in the α-phase in the scope of the Avrami equation, J. Mater. Sci. 45 (2010) 1328–1335. doi:10.1007/s10853-009-4086-3.

[14] V. Sencadas, R. Gregorio, S. Lanceros-Méndez, α to β phase transformation and microestructural changes of PVDF films induced by uniaxial stretch, J. Macromol. Sci. Part B Phys. 48 (2009) 514–525. doi:10.1080/00222340902837527.

[15] J. Gomes, J.S. Nunes, V. Sencadas, S. Lanceros-Mendez, Influence of the β-phase content and degree of crystallinity on the piezo-and ferroelectric properties of poly(vinylidene fluoride), Smart Mater. Struct. 19 (2010). doi:10.1088/0964-1726/19/6/065010.

[16] R. Gregorio, D.S. Borges, Effect of crystallization rate on the formation of the polymorphs of solution cast poly(vinylidene fluoride), Polymer. 49 (2008) 4009–4016. doi:10.1016/j.polymer.2008.07.010.

[17] V. Sencadas, C. Ribeiro, J. Nunes-Pereira, V. Correia, S. Lanceros-Méndez, Fiber average size and distribution dependence on the electrospinning parameters of poly(vinylidene fluoride-trifluoroethylene) membranes for biomedical applications, Appl. Phys. A Mater. Sci. Process. 109 (2012) 685-691. doi:10.1007/s00339-012-7101-5.

[18] H. Deplaine, J.L.G. Ribelles, G.G. Ferrer, Effect of the content of hydroxyapatite nanoparticles on the properties and bioactivity of poly(l-lactide) - Hybrid membranes, Compos. Sci. Technol. 70 (2010) 1805–1812. doi:10.1016/j.compscitech.2010.06.009.

[19] V.A. Santamaría, H. Deplaine, D. Mariggió, A.R. Villanueva-Molines, J.M. García-Aznar, J.L.G. Ribelles, M. Doblaré, G.G. Ferrer, I. Ochoa, Influence of the macro and micro-porous structure on the mechanical behavior of poly(l-lactic acid) scaffolds, J. Non. Cryst. Solids. 358 (2012) 3141–3149. doi:10.1016/j.jnoncrysol.2012.08.001.

[20] I. Izal, P. Aranda, P. Sanz-Ramos, P. Ripalda, G. Mora, F. Granero-Moltó, H. Deplaine, J.L. Gómez-Ribelles, G.G. Ferrer, V. Acosta, I. Ochoa, J.M. García-Aznar, E.J. Andreu, M. Monleón-Pradas, M. Doblaré, F. Prósper, Culture of human bone marrow-derived mesenchymal stem cells on of poly(L-lactic acid) scaffolds: potential application for the tissue engineering of cartilage., Knee Surgery, Sport. Traumatol. Arthrosc. 21 (2013) 1737–1750. doi:10.1007/s00167-012-2148-6.

[21] L.A. Turner, M. J. Dalby, Nanotopography-potential relevance in the stem cell niche, Biomater. Sci. 2 (2014) 1574–1594. doi:10.1039/c4bm00155a.

[22] R.J. McMurray, N. Gadegaard, P.M. Tsimbouri, K. V. Burgess, L.E. McNamara, R. Tare, K. Murawski, E. Kingham, R.O.C. Oreffo, M.J. Dalby, Nanoscale surfaces for the long-term maintenance of mesenchymal stem cell phenotype and multipotency,

Nat. Mater. 10 (2011) 637–644. doi:10.1038/nmat3058.

[23] J.C. Chang, S. Fujita, H. Tonami, K. Kato, H. Iwata, S.H. Hsu, Cell orientation and regulation of cell-cell communication in human mesenchymal stem cells on different patterns of electrospun fibers, Biomed. Mater. 8 (2013) 055002. doi:10.1088/1748-6041/8/5/055002.

[24] D.C.L. Rowland, T. Aquilina, A. Klein, O. Hakimi, P. Alexis-Mouthuy, A.J. Carr, S.J.B. Snelling, A comparative evaluation of the effect of polymer chemistry and fiber orientation on mesenchymal stem cell differentiation, J. Biomed. Mater. Res. - Part A. 104 (2016) 2843–2853. doi:10.1002/jbm.a.35829.

[25] M. Keremidarska, D. Gugutkov, G. Altankov, N. Krasteva, Impact of electrospun nanofibres orientation on mesenchymal stem cell adhesion and morphology, Comptes Rendus L'Academie Bulg. Des Sci. 68 (2015) 1271–1276.

[26] R. Sobreiro-Almeida, M. Tamaño-Machiavello, E. Carvalho, L. Cordón, S. Doria, L. Senent, D. Correia, C. Ribeiro, S. Lanceros-Méndez, R. Sabater i Serra, J. Gomez Ribelles, A. Sempere, Human Mesenchymal Stem Cells Growth and Osteogenic Differentiation on Piezoelectric Poly(vinylidene fluoride) Microsphere Substrates, Int. J. Mol. Sci. 18 (2017) 2391. doi:10.3390/ijms18112391.

[27] P.Y. Collart-Dutilleul, E. Secret, I. Panayotov, D. Deville De Périère, R.J. Martín-Palma, V. Torres-Costa, M. Martin, C. Gergely, J.O. Durand, F. Cunin, F.J. Cuisinier, Adhesion and proliferation of human mesenchymal stem cells from dental pulp on porous silicon scaffolds, ACS Appl. Mater. Interfaces. 6 (2014) 1719–1728. doi:10.1021/am4046316.

[28] Y.C. Kuo, S.C. Hung, S. hui Hsu, The effect of elastic biodegradable polyurethane electrospun nanofibers on the differentiation of mesenchymal stem cells, Colloids Surfaces B Biointerfaces. 122 (2014) 414–422. doi:10.1016/j.colsurfb.2014.07.017.

[29] J. Wu, L. Li, C. Fu, F. Yang, Z. Jiao, X. Shi, Y. Ito, Z. Wang, Q. Liu, P. Zhang, Micro-porous polyetheretherketone implants decorated with BMP-2 via phosphorylated gelatin coating for enhancing cell adhesion and osteogenic differentiation, Colloids Surfaces B Biointerfaces. 169 (2018) 233–241. doi:10.1016/j.colsurfb.2018.05.027.

[30] N. Li, G. Chen, J. Liu, Y. Xia, H. Chen, H. Tang, F. Zhang, N. Gu, Effect of surface

topography and bioactive properties on early adhesion and growth behavior of mouse preosteoblast MC3T3-E1 cells, ACS Appl. Mater. Interfaces. 6 (2014) 17134–17143. doi:10.1021/am5047944.

[31] B. Duan, H. Niu, W. Zhang, Y. Ma, Y. Yuan, C. Liu, Microporous density-mediated response of MSCs on 3D trimodal macro/micro/nano-porous scaffolds via fibronectin/integrin and FAK/MAPK signaling pathways, J. Mater. Chem. B. 5 (2017) 3586–3599. doi:10.1039/c7tb00041c.

[32] I.H. Jaafar, C.E. Leblon, M.T. Wei, D. Ou-Yang, J.P. Coulter, S.S. Jedlicka, Improving fluorescence imaging of biological cells on biomedical polymers, Acta Biomater. 7 (2011) 1588–98. doi:10.1016/j.actbio.2010.12.007.

[33] L. Qi, E.K. Knapton, X. Zhang, T. Zhang, C. Gu, Y. Zhao, Pre-culture Sudan Black B treatment suppresses autofluorescence signals emitted from polymer tissue scaffolds, Sci. Rep. 7 (2017) 8361. doi:10.1038/s41598-017-08723-2.

[34] T. Kawano, M. Sato, H. Yabu, M. Shimomura, Honeycomb-shaped surface topography induces differentiation of human mesenchymal stem cells (hMSCs): Uniform porous polymer scaffolds prepared by the breath figure technique, Biomater. Sci. 2 (2014) 52–56. doi:10.1039/c3bm60195a.

[35] C.H. Seo, K. Furukawa, K. Montagne, H. Jeong, T. Ushida, The effect of substrate microtopography on focal adhesion maturation and actin organization via the RhoA/ROCK pathway, Biomaterials. 32 (2011) 9568–9575. doi:10.1016/j.biomaterials.2011.08.077.

[36] C.S. Chen, J.L. Alonso, E. Ostuni, G.M. Whitesides, D.E. Ingber, Cell shape provides global control of focal adhesion assembly, Biochem. Biophys. Res. Commun. 307 (2003) 355–361. doi:10.1016/S0006-291X(03)01165-3.